# Optical measurements of faint LEO RSOs: Cubesats and Fengyun 1C Debris

**Peter Zimmer**
*J.T. McGraw and Associates, LLC*

**John T. McGraw**
*J.T. McGraw and Associates, LLC*

**Mark R. Ackermann**
*J.T. McGraw and Associates, LLC*

**ABSTRACT**

The first member satellites of the coming mega-constellations have launched, and over the next few years, LEO is going to get busy. Risks to new and existing missions are increasing geometrically. Optical observations can complement and augment radar surveillance, helping to derive and refine orbit elements, size and orientation estimates, and platform stability. Cued observations can refine these properties for known objects, while blind surveillance can discover new or lost objects. Small optical telescopes, strategically distributed across the globe, will perform as needed in both cued and blind observing modes. Each of these will contribute to space situational awareness (SSA) and space traffic management (STM) missions.

This paper builds on the work we demonstrated at last year's conference using a small, wide-field optical telescope to perform cued surveillance of various LEO objects. We extend that proof-of-concept work to a larger set of objects and observations, all with astrometry and photometry calibrated to GAIA DR2. The proof-of-concept work showed positive detections of fainter than 14th magnitude and sensitivity limits fainter than 15th magnitude, corresponding to diffuse black spheres of 10 cm and 6 cm diameter, respectively. There were, surprisingly, orientations of 1U cubesats that dropped below that threshold for a few seconds and, unsurprisingly, glints that were 10,000 times brighter than that. In the case of cubesats, there usually are images of the craft in the public domain, so some range of spacecraft pose can be considered in explaining brightness variation. Fengyun 1C debris, which pervades the sky, is notoriously difficult to detect optically, let alone measure, and the sizes and shapes of these pieces are completely unknown. Thus, the larger sample will help answer questions about the discrepancies between radar cross-section-derived sizes and optical signatures.

These observations will help constrain and refine models of expected photometric signals for LEO objects. Those models help inform the design and operation of optical telescope networks. This set of ongoing observations leads to the next step, which is routine operation of widely deployed systems automatically obtaining cued LEO observations.

## 1. INTRODUCTION

This year saw the mass deployment of the first members of the upcoming LEO mega-constellations. Across the various operators, there are plans for more than ten thousand new satellites in under a decade. Even this first mass deployment created a recent publicized STM incident [1]. A commensurate investment in SSA and STM has not been announced. LEO space is going to get busy fast. Even before the advent of these large-scale networks, there were not very many voices decrying an overabundance of SSA data. All sources of information on the positions, motions and disposition of these objects and their closest 20,000 neighbors will be critical to the "awareness" part of SSA and the "management" part of STM. Optical telescopes can assist in a cost-effective, agile and scalable way.

The work presented here demonstrates some of the ways optical telescopes can be used for SSA and STM missions and is a continuation of that presented at the 2018 AMOS Conference [2]. In that work, we observed several cubesats and Fengyun 1C (FY1C) debris with a prototype optical system partly from curiosity and as a test of new sCMOS detectors and detection techniques.

Sensitivity analysis gave us confidence that we would be able to readily detect the cubesats; pictures and diagrams abound for these systems. Still, we were surprised to find that two of the 1U cubesats could be become very faint. Clearly there are combinations of Sun phase angle and cubesat pose that present a very small optical signature.

Unsurprisingly, specular reflection caused rapid brightness increases often in excess of 5 magnitudes in a few hundred milliseconds. These features are very useful for deriving spin rates and ultimately can be used to assess shape and pose.

FY1C debris presents a different challenge. As fragments from a catastrophic disassembly, the shape and orientation of the objects are not known. Radar cross-section measurements (RCS) exist for the vast majority of the fragments, but they are all small enough to be in the awkward crossover region between Mie and Rayleigh scattering for the radar systems that likely produced the data. Area-to-mass ratios have been derived by [3] and [4], though that still leaves at least one too many unknown parameters that are required to work out their sizes.

We first attempted to observe FY1C debris with our earlier sensor systems that used interline CCDs [5]. Our simplistic models based on RCS values predicted that, although they were faint, we should have been able to detect them; we didn't; doing so became a challenge and goal for our work. These sensors were limited to exposure cadences of one frame per second (fps) or slower, requiring either large dead-time gaps between exposures or trailing losses to overwhelm the source signal. Combined with relatively low quantum efficiency, the sensitivity limits just were not adequate.

When we replaced those cameras with sCMOS systems, all the salient parameters improved: read noise, quantum efficiency and frame rate. We were able to measure three out of nine FY1C debris objects. One of them, NORAD #29948 with RCS of 0.08 $m^2$, was measured with a brightness within 0.2 magnitudes (brighter) of the model expected value, which is reasonable agreement given the model's simplicity. The other two pieces, 29796 (RCS of 0.044 $m^2$) and 30920 (RCS 0.0084 $m^2$) averaged 2.5 and 1.6 magnitudes fainter than expected. The remaining six objects had RCS values in between those two, and across multiple observations for each, they were undetected despite detection thresholds 3 – 4 magnitudes (16x – 40x) fainter than the model expectations. Two of those non-detections spanned nine attempts on each object.

That we missed some large fraction of them is not surprising, nor is the idea that these objects would be quite a bit fainter than expected. There is a truism among astronomers that it is a lot easier to make something fainter than you expect than brighter, be it stars, asteroids, supernovae, etc. We received very useful feedback on possible mechanisms at the 2018 AMOS conference, though no one effect seemed able to account for such a large deficit in light.

Therefore, we undertook the observations reported here, with the hope that more data might help. The next section will describe our updated detection system and the new observations. Section 3 summarizes the results for the cubesat and FY1C debris targets, and Section 4 will discuss a few of the possible explanations for why FY1C debris is so difficult to measure.

## 2. CUED OBSERVATIONS OF LEO OBJECTS

Because we were interested in observing cubesats and cataloged debris for which at least some physical properties are known, we obtained these observations in a cued observing mode. For cubesats, there are usually pictures or approximate size specifications from which to make some reasonable assumptions about how bright they should appear. For FY1C debris, we have legacy radar cross-section data. This means we can use the published TLEs to generate trajectories around which to search.

### 2.1. Upgraded detection system

Our current R&D system has been updated over the last year to incorporate a new optical system, new camera, and new mount. The current optical system is a 36 cm Celestron Rowe Ackermann Schmidt Astrograph (RASA) that operates at f/2.2. This system has a slightly longer focal length than our previous Hyperstar system, but the image quality and vignetting — and therefore overall throughput — is substantially improved.

The new sensor is a Finger Lakes Instruments (FLI) Kepler KL4040 sCMOS camera. The KL4040 has a 4096 x 4096 array of 9 um pixels. The sensor is frontside illuminated, so its peak quantum efficiency is above 70%, which is low compared to a backside illuminated device. The median read noise is just under 4 electrons RMS. Compared to the previous sensor, this is somewhat less sensitive, but that is more than compensated for by the KL4040's much larger physical area. This gives it a field of view of 7.15 square degrees when used with the RASA36. In addition, the KL4040 attaches to a GPS receiver that the camera uses to time stamp each image to within 20 us of UTC.

The new telescope mount is a Planewave L-350 direct drive mount operated in alt-az mode. This mount has a much faster slew rate and shorter settle time, reducing system deadtime. Coupled with the larger field of view of the optics, it is very effective at covering the sky.

**Figure 1 – The 0.35m Optical SSA system used for this work is located in north central New Mexico.**

### 2.2. The observations

We tasked the system to observe an ad hoc list of cubesats and FY1C debris that happened to pass over the site during twilight of 15 clear nights from June 8-28, 2019. Each observation consisted of 32 frames of 0.25 second exposure time each. When operating in alt-az mode, our system moves ahead of the objects' expected path based on the Space-Track [6] TLE. Unlike when operating our equatorially mounted systems, we stop the telescope motion rather than tracking the sidereal rate, because equatorial tracking with an alt-az system causes field rotation on the detector, and the linear motion of stars caused by not tracking is easier to compute.

The object then passes through the FOV such that if the TLE were perfectly accurate, the object would pass though the center of the FOV at the midpoint of the image stack. Larger objects in higher orbits are frequently very close to the point, but lower and smaller object can be shifted somewhat, though the vast majority are within a small fraction of the FOV of the center. With this configuration, our effective search area per observation covers many tens of kilometers both along- and cross-track, quite a bit larger than most TLE errors.

We process the resulting imagery to remove instrumental signatures analogous to bias and dark corrections, which have been modified from standard CCD reduction procedures to account for sCMOS sensor architectural differences. Stars in the images are detected, measured and suppressed. The residual frames are processed through JTMA's streak detection pipeline [7] to find objects matching the expected rates for the target TLE.

### 2.3. Photometric model estimates of satellite intensity.

We compare the resulting measured object intensities to a simple model that we described in our previous work [1], with a small modification of a slightly lower estimated albedo of 0.13 instead of 0.16 to be better in line with other work in the SSA community [8]. For the FY1C debris objects, we continue to use the measured radar cross sections to estimate size, which is corrected for Mie scattering effect because the objects are similar in size to the radar wavelength. For the cubesats, we use size estimates based on the cubesat form factor, generating estimated magnitudes

for both a maximum and minimum viewing aspect at the observed solar phase angle. For the majority of the observations, the solar phase angle was in the range of 65 – 75 degrees and the range to the object is taken from the TLE generated ephemeris.

## 3. SUMMARY OF RESULTS

Measurements of the observed objects and their estimated intensity both referenced to the GAIA photometric system [9]. For the purposes of this report, we offer a concise summary of the objects, their range of measured brightness, and the expected magnitude based on the simple model. Anyone interested in more detailed results for specific objects is encouraged to contact the authors.

### 3.1. Cubesats

We observed a total of 25 cubesats spanning a size range of 0.5U to 6U, all of which were detected at least once. Several were observed on multiple nights. We've also included four cubesats from our previous work in 2018 for completeness. Table 1 shows a summary of the objects, their range at observation, their measured magnitude range, and their expected brightness based on our simple model. No model results were computed for the three 6U cubesats because they each had complicated geometries of deployed solar panels and instruments that obviously ran counter to our model technique. We also include some observations of Starlink satellites taken just a few weeks after launch during a few fortunate passes, because these objects are of some current interest.

The overall results are not surprising. The cubesats generally fell within the expected brightness range, save for two of the satellites from the 2018 work: Cute 1 Co-55 and NEE-02. Both of these objects, while detected well in some observation sets, dropped below our detection threshold in others. And in both cases, they are 1U cubesats with deployed solar arrays. Our best explanation for these dramatic darkened periods is that the solar panel is self-shadowing itself and the craft. None of the other 1U craft appear to have deployed panels, though that fact has not been proved conclusively. Aside from those instances, we reliably detect and monitor cubesats as small as 0.5U.

| Name | Size | RCS ($m^2$) | Range (km) | Max (mag) | Min (mag) |
|---|---|---|---|---|---|
| AEROCUBE 7B | 1.5U | | 580 | 10.8 | 12.4 |
| AEROCUBE 7C | 1.5U | | 580 | 6.0 | 12.6 |
| | | | | | |
| CUTE 1 CO-55 | 1U | 0.08 | 1003 | 7.5 | 15.4 |
| ROBUSTA-1B | 1U | | 620 | 12.0 | 13.4 |
| SEEDS 2 | 1U | 0.049 | 625 | 10.0 | 14.5 |
| SKCUBE | 1U | | 542 | 10.8 | 12.0 |
| NEE-02 | 1U | 0.019 | 915 | 14.2 | 15.4 |
| 1KUNS-PF | 1U | | 400 | 10.1 | 12.8 |
| EQUISAT | 1U | | 544 | 8.9 | 9.8 |
| | | | | | |
| AEROCUBE 6B | 0.5U | | 770 | 13.1 | 13.3 |

**Table 1a – This table summarizes our measurements of 0.5 – 1.5 U cubesats. RCS measurements stopped being routinely published a few years ago when cubesats first started to be launched; therefore only a few have measured values. Range is based on the TLE generated ephemeris positions, and the Max and Min values are measured magnitudes referenced to GAIA DR2.**

| Name | Size | Range (km) | Max (mag) | Min (mag) |
|---|---|---|---|---|
| CUBERRT | 6U | 423 | 9.5 | 9.6 |
| RAINCUBE | 6U | 560 | 9.0 | 9.2 |
| HALOSAT | 6U | 510 | 9.7 | 10.2 |
| | | | | |
| Ex-Alta 1 | 3U | 401 | 4.6 | 10.5 |
| STF-1 | 3U | 890 | 11.2 | 13.3 |
| AALTO 1 | 3U | 715 | 9.3 | 12.6 |
| SHIELDS-1 | 3U | 545 | 8.9 | 8.9 |
| LITHUANICASAT-2 | 3U | 590 | 8.5 | 10.3 |
| DIAMOND GREEN | 3U | 590 | 10.4 | 11.1 |
| DIAMOND BLUE | 3U | 545 | 11.0 | 11.1 |
| DIAMOND RED | 3U | 605 | 10.2 | 12.7 |
| AEROCUBE 12B | 3U | 780 | 11.1 | 12.3 |
| ASGARDIA 1 | 3U | 501 | 11.0 | 11.1 |
| PEGASUS | 3U | 550 | 11.6 | 11.9 |
| | | | | |
| VZLUSAT 1 | 2U | 600 | 10.9 | 11.7 |
| UCLSAT | 2U | 628 | 11.4 | 12.2 |
| COMPASS 2 | 2U | 580 | 8.8 | 10.5 |
| NUDTSAT | 2U | 515 | 11.1 | 11.5 |

| Name | | Range (km) | Max (mag) | Min (mag) |
|---|---|---|---|---|
| OBJECT A | Starlink | 640 | 4.9 | 5.4 |
| OBJECT B | Starlink | 749 | 9.6 | 10.4 |
| OBJECT J | Starlink | 680 | 10.8 | 11.8 |
| OBJECT Y | Starlink | 640 | 4.1 | 4.7 |
| OBJECT AZ | Starlink | 780 | 4.2 | 4.6 |
| OBJECT PE | Starlink | 524 | 11.9 | 12.6 |
| OBJECT PD | Starlink | 450 | 12.5 | 12.6 |
| OBJECT PJ | Starlink | 497 | 8.5 | 9.5 |

**Tables 1b and 1c – Same information as Table 1a, except with 2U – 6U objects and Starlink member objects, respectively.**

### 3.2. Fengyun 1C (FY) Debris

At any time, over any observing site, the plurality of known objects moving overhead is debris from the 2007 FY antisatellite missile test [18]. FY debris represents a relevant and challenging test for optical LEO observations. Although radar cross-sections are publicly available for most of these objects, very little is known about their size, shape, material, color, or orientation. Figure 2 shows a picture of the Fengyun 1C weather satellite on the ground. Prior to its destruction, the RCS of FY1C was 2.5 $m^2$; it is now 0.25 $m^2$. A few of the other pieces exceed 0.1 $m^2$ as shown in Figure 3, while the remainder are much smaller following the expected power law for on-orbit fragmentation. Based on this, it seems likely that the majority of the fragments are from the solar panels.

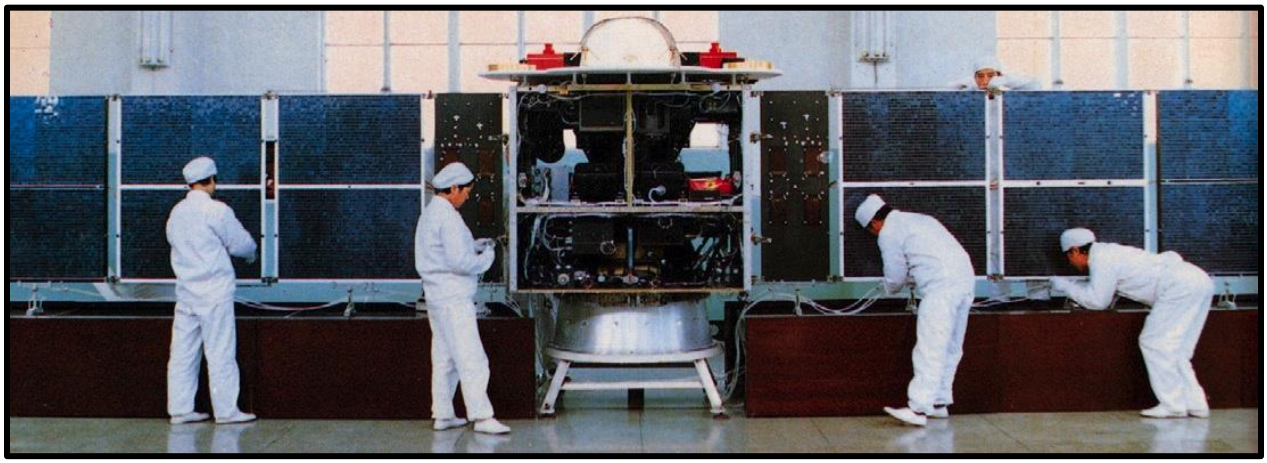

**Figure 2 – This picture shows FY1C on the ground with human technicians for scale. (Courtesy: NASA's Orbital Debris Quarterly News)**

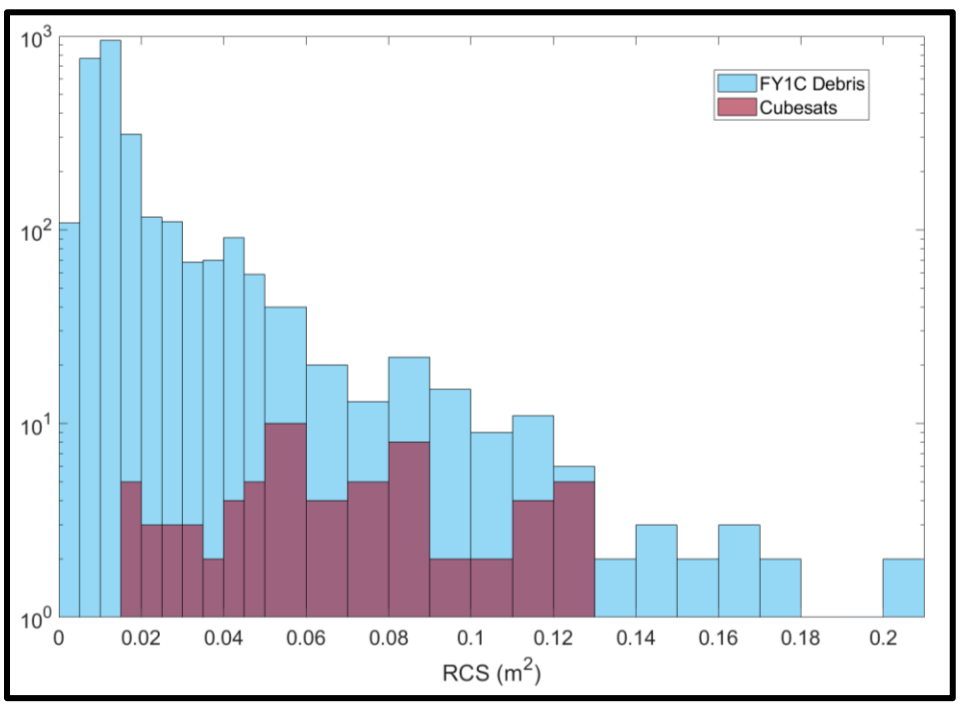


**Figure 3 – This histogram shows the measured RCS values for cataloged FY1C debris. Note the change in bin size for the smaller values – only two digits of significance are reported for the RCS values, and there are many more small pieces. RCS values for cubesats, where reported, are shown for comparison.**

We attempted 342 observations of 144 FY1C debris objects that passed overhead during our observing period, chosen only for being at favorable elevation and sun angle, with typically two observations per object per pass. Of these, 34 different objects were detected across 71 of the observations. Upper limits on brightness are placed on the rest. Figure 4 shows a comparison between the expected and the measured brightness as a function of RCS. The detection rate is not obviously a function of the RCS. Table 2 summarizes the detections. One object, NORAD 30050, was observed separately on three different nights, and the measurements are consistent within 10% of each other when accounting for range and phase variations.

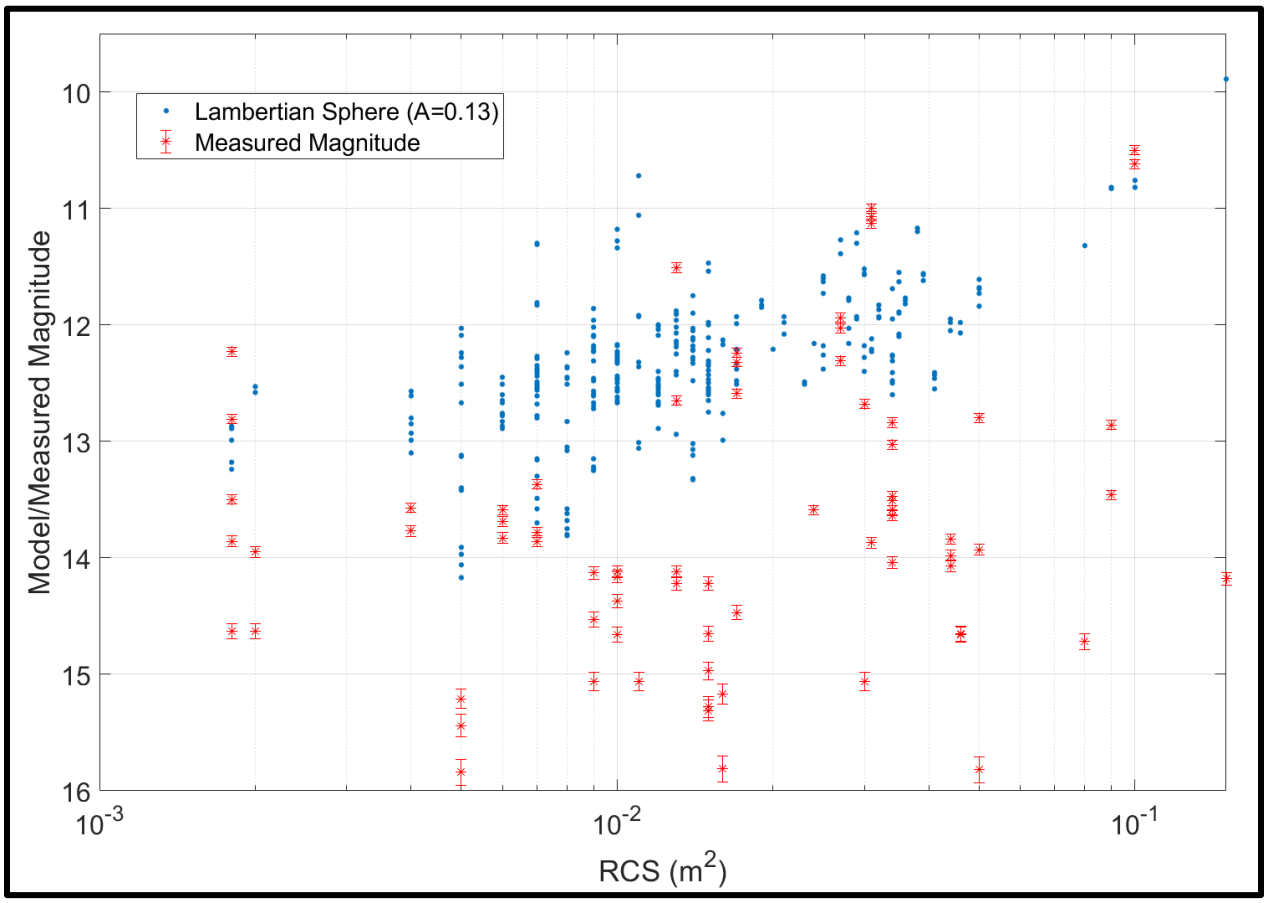


**Figure 4 – The blue dots show the expect magnitude of the objects for all the observations plotted against their RCS. The red asterisks are the measured values with their associated error estimates. No systematic effect with RCS is apparent. Objects with both large and small RCS values are detected.**

The difference between the measured brightness and upper limits of these fragments and the expected values are larger than anticipated but consistent with what we saw in our earlier sample. Our detection thresholds are typically in the range of magnitude 15.5 - 15.9. FY1C debris is systematically fainter than expected usually by 2 - 4 magnitudes. Either these fragments are much blacker than the model assumes, smaller than reported by RCS, or the TLE positions very much in error. Each of these potential explanations have interesting implications and, in the context of these new observations, we'll explore some of those possibilities further in Section 4.

## 4. ONGOING EXPERIMENTS

These observations confirm what our previous work showed, though now with a much more substantial sample size, N=142 vs. N=9. Figure 5 shows a histogram of observed minus model brightness values. The detected objects are typically 1 - 2 magnitudes fainter than expected, which is similar to our results from cubesat measurements. Cubesat can show dramatic decreases in brightness, presumably due to self-shadowing. However, those objects also show similarly large increases in brightness. Therefore missing a few unfavorably oriented objects is to be expected.

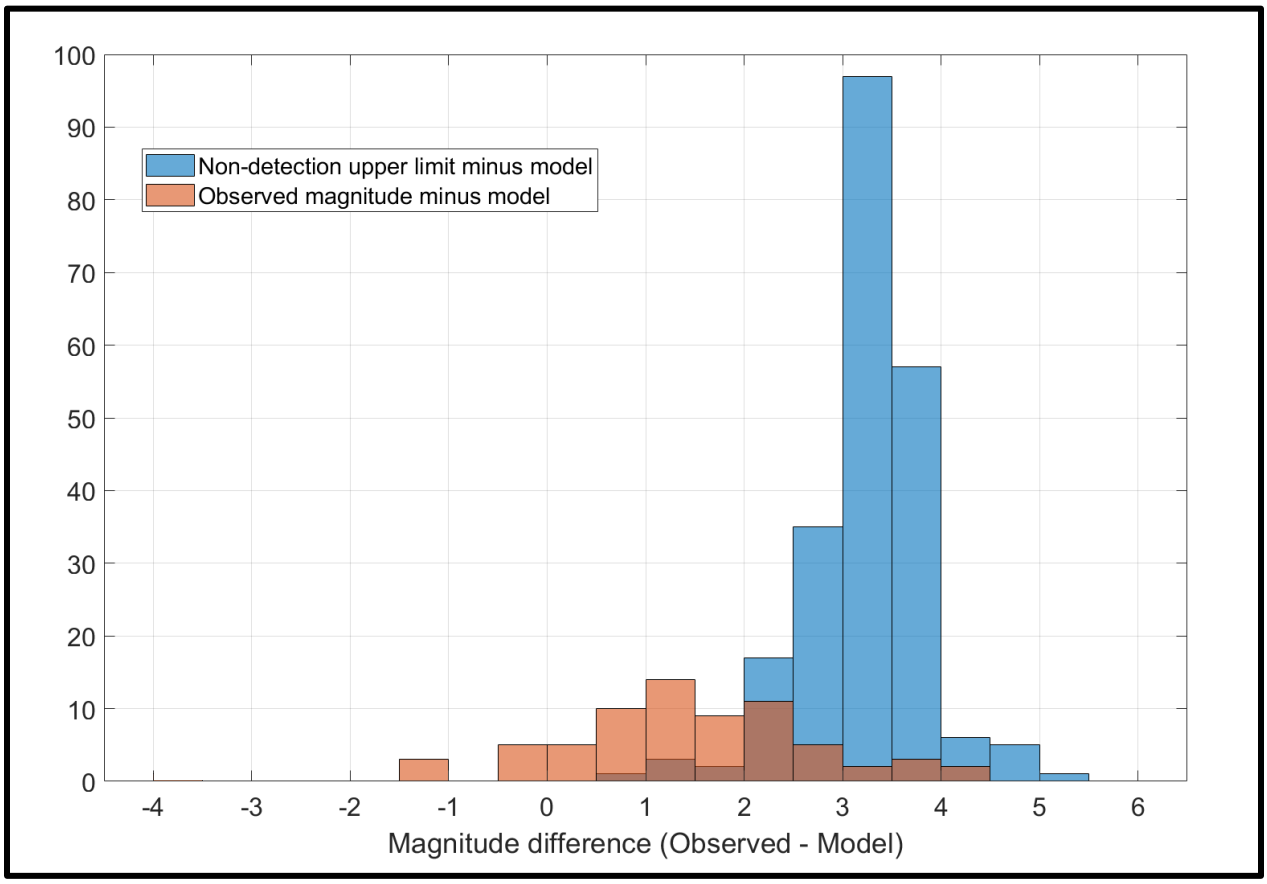


**Figure 5 – This histogram shows the observed minus model values for both the detected objects, in orange, and the non-detection upper limits in blue.**

For FY1C debris though, we see most objects are at least 2.5 magnitudes or more fainter than expected based on the non-detection limits. Approximately 75% are not detected at all. As mentioned before, astronomers know that it is much easier to make something appear fainter than it is to make it appear brighter. But differences this large are a bit more challenging. So far, no one explanation seems to be able to cover that deficit, but invoking multiple mechanisms is always fraught.

Of the explanations that we proposed last year, we can eliminate some. The possibility that it is errors in the TLE positions is ruled out. TLEs after the observations are nearly identical, and the FOV of our new system is substantially larger than last year. If TLEs were the issue, we'd at least see a larger fraction of objects detected. We also posited that perhaps the explosion of the ASAT might have coated the fragments with carbon or other black material. We have since learned that the ASAT was a kinetic warhead, not an explosive, and while it may have caused thruster fuel to escape, it would be difficult to believe that it would have made all the pieces that black.

Some remaining possibilities are:

- Lower albedo: The assumed albedo of 13% is based on measurements of exterior surfaces. The ASAT disruption assuredly would have exposed interior parts, many of which might have been painted black as is common in satellites with optical sensors.
- Carbon fiber construction: Carbon fiber fragments are very black and can often be quite needle-like in shape. Radar reflectivity of those fragments will not be appreciable, though, unless the fragment is large.
- RCS values: Systematic effects in reported RCS values could cause the inferred linear size to be systematically overestimated. For instance, if the RCS values are a maximum observed during a pass or over several passes, they might be biased compared to when we happened to observe. The RCS measurements are not well documented, so a fair bit of uncertainty can be assigned here, though multiple factors of 10 would seem unlikely.
- Self-shadowing: We've seen that cubesats can get much fainter than average for short periods. This is attributed to self-shadowing, where the illuminated portion of the object is not visible. Geometries such as a flat plate with a surface normal pointing 90 degrees from the line of sight through 90 plus the Sun phase angle could be very dark, with only narrow edges lit. A random distribution of flat-plate orientations would lead to about 30 - 40% of the objects we observed to be missing. Given that many of the fragments are solar panel pieces, this might explain a large fraction of non-detections.
- Non-random orientations: These fragments have been tumbling for 12 years, making in excess of 50,000 revolutions. That is a lot of time to couple the drag forces with tumbling. Is it possible that these things have a preferred orientation, perhaps along the direction of motion, that when coupled with self-shadowing, makes them difficult to see in terminator illumination conditions? Among the things we will look at further are the estimates of area-to-mass ratio for FY1C debris based on the time evolution of their orbit.

There are, without doubt, many more possible and plausible mechanisms. For once though, the authors are pleased to not end a paper with "we need more data." But rather, this curious mystery continues. More data on FY1C objects will be acquired as these observations move from R&D to operational systems. That may help solve this issue, but even so, ore detailed models and better understanding of the interplay between optical brightness and RCS are needed.

| Date (UTC) | NORAD ID | RCS ($m^2$) | Size (m) | Rate (”/sec) | Range (km) | Phase (deg) | Model (mag) | Measured (mag) |
|---|---|---|---|---|---|---|---|---|
| 6/11/2019 | 29891 | 0.09 | 0.23 | 1758 | 874 | 67.35 | 10.82 | 12.86 |
| 6/11/2019 | 29891 | 0.09 | 0.23 | 1794 | 866 | 68.61 | 10.83 | 13.46 |
| 6/12/2019 | 29988 | 0.15 | 0.37 | 1798 | 852 | 72.61 | 9.89 | 14.18 |
| 6/8/2019 | 30050 | 0.034 | 0.15 | 1247 | 1159 | 68.94 | 12.41 | 13.03 |
| 6/8/2019 | 30050 | 0.034 | 0.15 | 1144 | 1215 | 68.25 | 12.50 | 12.84 |
| 6/12/2019 | 30050 | 0.034 | 0.15 | 1289 | 1172 | 71.15 | 12.48 | 13.51 |
| 6/12/2019 | 30050 | 0.034 | 0.15 | 1258 | 1189 | 70.42 | 12.50 | 13.47 |
| 6/22/2019 | 30050 | 0.034 | 0.15 | 1470 | 1032 | 74.22 | 12.27 | 13.59 |
| 6/22/2019 | 30050 | 0.034 | 0.15 | 1461 | 1037 | 73.30 | 12.26 | 14.04 |
| 6/22/2019 | 30050 | 0.034 | 0.15 | 1386 | 1068 | 72.60 | 12.31 | 13.64 |
| 6/22/2019 | 30078 | 0.1 | 0.26 | 1621 | 915 | 72.96 | 10.82 | 10.62 |
| 6/22/2019 | 30078 | 0.1 | 0.26 | 1742 | 881 | 74.00 | 10.76 | 10.50 |
| 6/22/2019 | 30109 | 0.046 | 0.16 | 1300 | 1076 | 68.70 | 12.07 | 14.66 |
| 6/22/2019 | 30109 | 0.046 | 0.16 | 1435 | 1020 | 69.72 | 11.98 | 14.65 |
| 6/22/2019 | 30115 | 0.05 | 0.17 | 1496 | 955 | 72.69 | 11.84 | 12.80 |
| 6/22/2019 | 30115 | 0.05 | 0.17 | 1670 | 900 | 73.73 | 11.73 | 13.93 |
| 6/22/2019 | 30115 | 0.05 | 0.17 | 1779 | 871 | 74.81 | 11.69 | 15.82 |
| 6/22/2019 | 30150 | 0.044 | 0.16 | 1559 | 986 | 70.46 | 11.95 | 14.07 |
| 6/22/2019 | 30150 | 0.044 | 0.16 | 1496 | 1008 | 69.67 | 11.98 | 13.98 |
| 6/22/2019 | 30150 | 0.044 | 0.16 | 1385 | 1052 | 68.97 | 12.05 | 13.84 |
| 6/20/2019 | 30174 | 0.08 | 0.21 | 1528 | 1001 | 66.52 | 11.32 | 14.72 |
| 6/9/2019 | 30239 | 0.031 | 0.15 | 1102 | 1424 | 67.31 | 12.23 | 11.13 |
| 6/9/2019 | 30239 | 0.031 | 0.15 | 1095 | 1427 | 66.52 | 12.21 | 11.00 |
| 6/9/2019 | 30239 | 0.031 | 0.15 | 1062 | 1449 | 65.71 | 12.23 | 11.07 |
| 6/11/2019 | 30261 | 0.027 | 0.14 | 1983 | 730 | 63.23 | 11.39 | 12.03 |
| 6/11/2019 | 30261 | 0.027 | 0.14 | 2265 | 682 | 64.48 | 11.27 | 11.94 |
| 6/11/2019 | 30261 | 0.027 | 0.14 | 2313 | 676 | 65.84 | 11.27 | 12.31 |
| 6/20/2019 | 30308 | 0.013 | 0.13 | 1996 | 783 | 68.90 | 11.91 | 12.65 |
| 6/20/2019 | 30308 | 0.013 | 0.13 | 1878 | 810 | 68.05 | 11.96 | 11.51 |
| 6/22/2019 | 30526 | 0.031 | 0.15 | 1636 | 930 | 75.47 | 12.12 | 13.87 |
| 6/12/2019 | 30556 | 0.017 | 0.13 | 1267 | 1045 | 70.21 | 12.48 | 12.59 |
| 6/12/2019 | 30556 | 0.017 | 0.13 | 1463 | 967 | 71.21 | 12.33 | 12.32 |
| 6/12/2019 | 30556 | 0.017 | 0.13 | 1639 | 907 | 72.26 | 12.21 | 12.24 |
| 6/9/2019 | 30646 | 0.03 | 0.15 | 1498 | 1016 | 67.08 | 11.52 | 12.68 |
| 6/9/2019 | 30646 | 0.03 | 0.15 | 1537 | 1002 | 68.21 | 11.52 | 15.06 |
| 6/20/2019 | 30702 | 0.007 | 0.12 | 1379 | 1004 | 67.37 | 12.61 | 13.37 |
| 6/20/2019 | 30702 | 0.007 | 0.12 | 1564 | 939 | 68.44 | 12.49 | 13.78 |
| 6/12/2019 | 30879 | 0.0018 | 0.09 | 1433 | 1021 | 70.69 | 13.24 | 12.81 |
| 6/12/2019 | 30879 | 0.0018 | 0.09 | 1536 | 982 | 71.74 | 13.18 | 12.23 |

| | | | | | | | | |
|---|---|---|---|---|---|---|---|---|
| 6/22/2019 | 30879 | 0.0018 | 0.09 | 1603 | 905 | 71.10 | 12.99 | 13.50 |
| 6/22/2019 | 30879 | 0.0018 | 0.09 | 1783 | 856 | 72.20 | 12.89 | 13.86 |
| 6/22/2019 | 30879 | 0.0018 | 0.09 | 1864 | 838 | 73.40 | 12.87 | 14.63 |
| 6/12/2019 | 30924 | 0.024 | 0.14 | 1652 | 942 | 71.68 | 12.16 | 13.59 |
| 6/22/2019 | 31069 | 0.017 | 0.13 | 1790 | 842 | 69.33 | 11.99 | 14.47 |
| 6/22/2019 | 31072 | 0.016 | 0.13 | 1057 | 1291 | 71.83 | 12.99 | 15.81 |
| 6/22/2019 | 31072 | 0.016 | 0.13 | 1251 | 1178 | 70.33 | 12.76 | 15.17 |
| 6/22/2019 | 31389 | 0.006 | 0.11 | 1372 | 1071 | 68.99 | 12.83 | 13.59 |
| 6/22/2019 | 31389 | 0.006 | 0.11 | 1480 | 1028 | 70.11 | 12.77 | 13.69 |
| 6/22/2019 | 31389 | 0.006 | 0.11 | 1532 | 1011 | 71.19 | 12.76 | 13.83 |
| 6/22/2019 | 31813 | 0.015 | 0.13 | 2409 | 656 | 68.53 | 11.47 | 15.28 |
| 6/22/2019 | 32110 | 0.015 | 0.13 | 1603 | 902 | 71.14 | 12.22 | 15.31 |
| 6/9/2019 | 32133 | 0.01 | 0.12 | 1417 | 1019 | 63.38 | 12.65 | 14.37 |
| 6/9/2019 | 32133 | 0.01 | 0.12 | 1561 | 969 | 64.57 | 12.56 | 14.12 |
| 6/15/2019 | 32136 | 0.009 | 0.12 | 1554 | 923 | 69.58 | 12.67 | 14.13 |
| 6/20/2019 | 32406 | 0.011 | 0.13 | 2657 | 509 | 70.81 | 11.06 | 15.06 |
| 6/12/2019 | 32464 | 0.01 | 0.12 | 1748 | 872 | 71.76 | 12.28 | 14.66 |
| 6/12/2019 | 32464 | 0.01 | 0.12 | 1653 | 900 | 70.14 | 12.32 | 14.16 |
| 6/9/2019 | 33650 | 0.005 | 0.11 | 994 | 1401 | 67.42 | 14.17 | 15.44 |
| 6/9/2019 | 33650 | 0.005 | 0.11 | 1075 | 1342 | 66.58 | 14.06 | 15.84 |
| 6/9/2019 | 33650 | 0.005 | 0.11 | 1143 | 1296 | 65.70 | 13.97 | 15.21 |
| 6/11/2019 | 35223 | 0.002 | 0.09 | 1936 | 800 | 64.38 | 12.53 | 14.63 |
| 6/11/2019 | 35223 | 0.002 | 0.09 | 1906 | 807 | 65.67 | 12.58 | 13.95 |
| 6/15/2019 | 35234 | 0.007 | 0.12 | 2119 | 740 | 72.95 | 12.54 | 13.86 |
| 6/11/2019 | 35239 | 0.004 | 0.11 | 1254 | 1140 | 62.96 | 12.99 | 13.77 |
| 6/11/2019 | 35239 | 0.004 | 0.11 | 1126 | 1207 | 62.17 | 13.10 | 13.57 |
| 6/9/2019 | 36247 | 0.009 | 0.12 | 1128 | 1263 | 62.76 | 13.22 | 14.53 |
| 6/9/2019 | 36247 | 0.009 | 0.12 | 1218 | 1211 | 63.92 | 13.15 | 15.06 |
| 6/22/2019 | 36676 | 0.013 | 0.13 | 1638 | 888 | 68.09 | 12.16 | 14.22 |
| 6/22/2019 | 36676 | 0.013 | 0.13 | 1805 | 844 | 68.87 | 12.07 | 14.12 |
| 6/22/2019 | 41006 | 0.015 | 0.13 | 1550 | 979 | 72.63 | 12.43 | 14.97 |
| 6/22/2019 | 41006 | 0.015 | 0.13 | 1652 | 947 | 71.96 | 12.34 | 14.65 |
| 6/22/2019 | 41006 | 0.015 | 0.13 | 1666 | 943 | 71.28 | 12.32 | 14.22 |

**Table 2 – This table summarizes the FY1C observations reported in this work. The size column is the estimated object diameter based on the NASA [9] model. Rate, range, and phase values are based on TLE generated ephemeris. The model magnitude is from our simple Lambertian sphere model described in Section 2.3, and the measured value is calibrated to GAIA DR2 G-band values.**

## REFERENCES


[1] STM incident

[2] P. Zimmer, J. T. McGraw, and M. R. Ackermann, "Real-time Optical Space Situational Awareness of Low-Earth Orbit with Small Telescopes," in *Advanced Maui Optical and Space Surveillance (AMOS) Technologies Conference*, 2018.

[3] C. Pardini and L. Anselmo, "Evolution of the debris cloud generated by the Fengyun-1C fragmentation event," in *International Symposium on Space Flight Dynamics*, 2007.

[4] J. V. Lambert, "Fengyun-1C Debris Cloud Evolution Over One Decade," in *Advanced Maui Optical and Space Surveillance (AMOS) Technologies Conference*, 2018.

[5] P. Zimmer, J. McGraw, and M. Ackermann, "Real-Time Optical Surveillance of LEO/MEO with Small Telescopes," in *Advanced Maui Optical and Space Surveillance Technologies Conference*, 2015, p. 103.

[6] https://space-track.org

[7] P. Zimmer, J. McGraw, and M. Ackermann, "Towards Routine Uncued Surveillance of Small Objects at and near Geostationary Orbit with Small Telescopes," in *Advanced Maui Optical and Space Surveillance Technologies Conference*, 2017.

[8] M. Mulrooney, M. Matney, M. Hejduk, and E. Barker, "An Investigation of Global Albedo Values," in *Advanced Maui Optical and Space Surveillance Technologies Conference*, 2008, p. E65.

[9] Gaia Collaboration *et al.*, "The Gaia mission," *Astron. Astrophys.*, vol. 595, p. A1, Nov. 2016.

[10] R. Lambour, T. Morgan, and N. Rajan, "Orbital debris size estimation from radar cross section measurements," in *Proceeding of the 2000 Space Control Conference*, 2000.